Electronic Supplementary Material (ESI) for Journal of Materials Chemistry A.
This journal is © The Royal Society of Chemistry 2018

Electronic Supplementary Information

Defects-rich $MoS_{2(1-x)}Se_{2x}$ few layers nanocomposites: a superior anode material for high-performance lithium-ion batteries

Guohui Cai, Lei Peng, Shiyong Ye, Yucheng Huang, Guangfeng Wang* Xiaojun Zhang*

†Key Laboratory of Chem-Biosensing, Anhui province; Key Laboratory of Functional Molecular Solids, Anhui province; College of Chemistry and Materials Science, Anhui Normal University, Wuhu 241000, P. R. China

Experimental section

Materials and reagents

Sodium molybdate dihydrate ($Na_2MoO_4.2H_2O$), Thiourea (NH_2CSNH_2), Selenium dioxide (SeO_2), Sodium borohydride ($NaBH_4$),Hydrochloric acid (36%-38%), Polyvinylidene fluoride(PVDF), All reagents were of analytical grade, and used without further purification. Deionized water was supplied with a Millipore Water System (18.25 MΩ cm).

Synthesis of pure inorganic MoO_3 nanowires

The pure inorganic MoO_3 nanowires were synthesized via a simple hydrothermal method. In detail, 200 mM of $Na_2MoO_4.2H_2O$ was dissolved in 70 mL deionized water with magnetic stirring for 30 min. Under vigorously stirring, 5 mL of Hydrochloric acid was slowly added into the solution of $Na_2MoO_4.2H_2O$ stirring for another 30 min. The mixed solution was then transferred into a Teflon-lined autoclave with 100 mL capacity and maintained at 180 ℃ for

24 h. After that, the product was collected by centrifugation, and then thoroughly washed three times with water and ethanol.

Synthesis of the $MoS_{2(1-x)}Se_{2x}$ nanosheets

The $MoS_{2(1-x)}Se_{2x}$ hybrid was synthesized using the as-prepared pure inorganic MoO_3 nanowires as precursors. 40 mM MoO_3 powder was dispersed in the 70mL deionized water with magnetic stirring for 30 min. Then, 1 mL of Hydrochloric acid was slowly added into the solution of MoO_3 stirring for another 30 min. Successively, 60mM of thiourea and 20 mM SeO_2 and 80 mM $NaBH_4$ was sequentially added to the homogeneous dispersion which was then transferred to a Teflon-lined stainless-steel autoclave and treated at 180 ℃for 24 h. The $MoS_{2(1-x)}Se_{2x}$ product was collected by centrifugation and washed with deionized water and ethanol several times and dried in a vacuum oven at 60 ℃ overnight.

Synthesis different selenium-sulfur ratios of the $MoS_{2(1-x)}Se_{2x}$ nanosheets

The synthesis method of different selenium-sulfur ratios of the $MoS_{2(1-x)}Se_{2x}$ nanosheets that of Synthesis $MoS_{2(1-x)}Se_{2x}$. Only changed the concentration of thiourea and selenium dioxide.

Structural characterization

The phase purities of the samples were characterized by X-ray diffraction (Bruker D8ADVANCE) with irradiation from a Cu target (Kα, λ =0.15406 nm) under a voltage of 40 KV and a current of 40 mA. The morphologies and sizes of the sample were observed by a field-emission scanning electron microscopy (FESEM, Hitachi S-4800,5 KV) and transmission electron microscope (TEM, Hitachi HT-7700, 120 KV). X-ray energy dispersive spectroscopy (EDS) was obtained on FESEM. High-resolution transmission electron X-ray

energy dispersive microscopy (HRTEM) images were obtained using a transmission electron microscopy (TEM,FEI TECNAI-G2 200 kV). The Brunauer-Emmett-Teller (BET) tests were determined via a surface analyzer (Micromeritics ASAP 2460). All the as-prepared samples were degassed at 120 °C for 6 hprior to nitrogen adsorption measurements. Laser Raman spectroscopy (Renishaw inVia). X-ray photoelectron spectroscopy (XPS) measurements are performed on an ESCALAB 250 spectrometer (Perkin-Elmer) to characterize the surface chemical composition. The source gun type of the XPS was Al Kα.

Electrochemical measurements

For LIBs test, the sample, conductive carbon black and PVDF as a binder were mixed thoroughly in a weight ratio of 8:1:1. The slurry was coated on copper foil and dried in a vacuum oven at 80 °C overnight. The electrolyte was composed of 1 M $LiPF_6$ in a mixture of ethylene carbonate, diethyl carbonate (EC: DEC=1: 1, in volume). Electrochemical experiments were performed using 2032-type coin cells with Li reference electrode, which were assembled in an argon-filled glove box (Mikrouna, Super (1220/750/900). The galvanostatic discharge-charge characteristics were tested between the potentials of 0.01 and 3.0 V using a Neware battery tester. Cyclic voltammetry (CV, scanning rate of 0.1 mV s^{-1}) and electrochemical impedance spectroscopy (EIS, frequency range from 0.01 Hz to 100 kHz) were tested on a CHI 760D electrochemical workstation.

Computational Methods

First-principles calculations were performed in the framework of density functional theory (DFT) as implemented in the Vienna ab initio simulation package (VASP).[16,17] The electron-ion interactions were described by the projector-augmented plane wave (PAW) method.[18]

The generalized gradient approximation (GGA) was used for the exchange-correlation functional with the Perdew-Burke-Ernzerhof (PBE) parameterization.[19,20] The cutoff energy for the plane-wave basis was set to 400 eV. The convergence thresholds were set to 10^{-5} eV and 10^{-2} eV/Å for energy and force, respectively. Vacuum height was set to 15 Å along z direction to avoid the interactions between two periodic repeating units. The Brillouin zone was represented by a Monkhorst−Pack[21] special k-point mesh of 5×5×1 for geometry optimizations, whereas a larger grid of 7×7×1 was used for band structure computations.

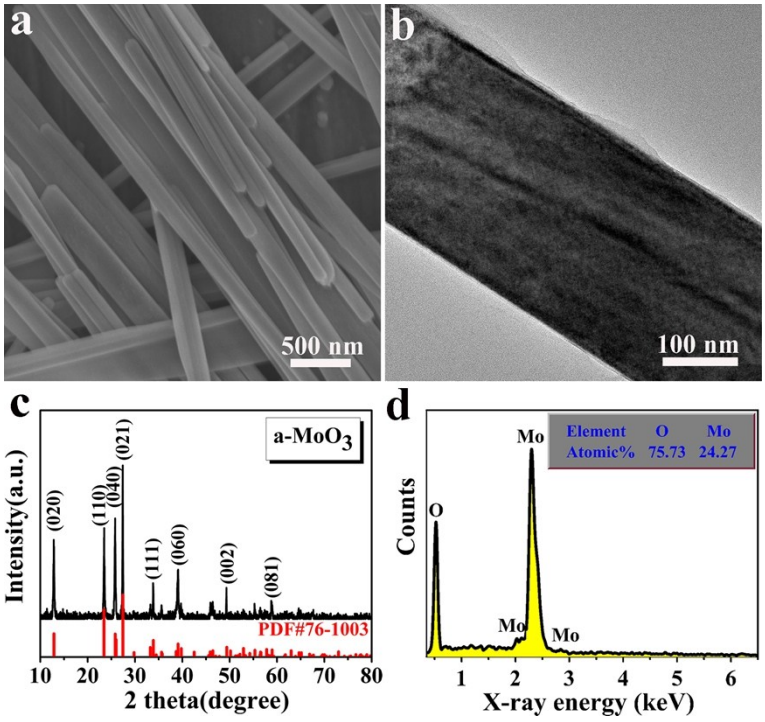

Figure S1 a,b) FESEM and HRTEM images, c,d) XRD and EDX pattern of the MoO_3 nanorods.

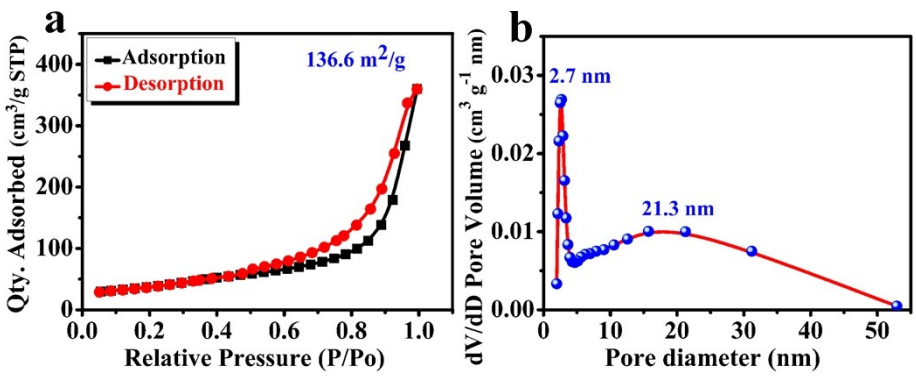

Figure S2 a,b) N_2 adsorption/desorption isotherm and the corresponding pore-size distribution plot of the $MoS_{2(1-x)}Se_{2x}$ (x=0.25) nanosheets.

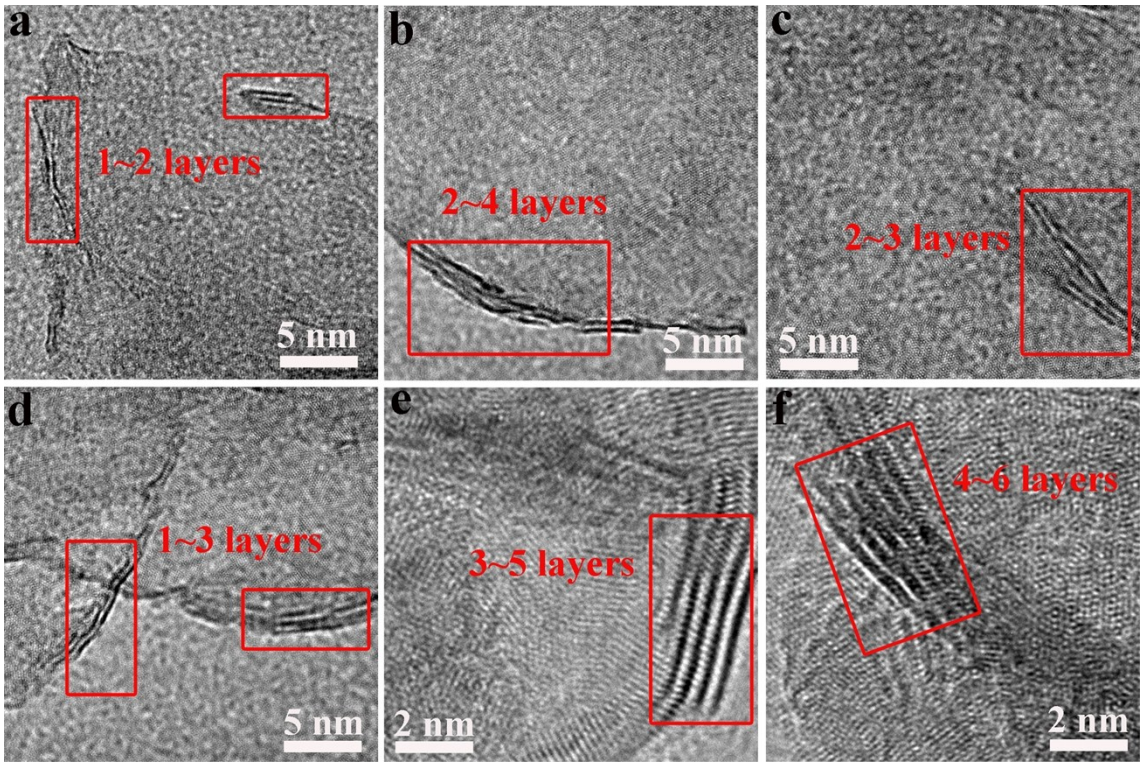

Figure S3 a-f) HRTEM showing different layers of the $MoS_{2(1-x)}Se_{2x}$ (x=0.25) nanosheets.

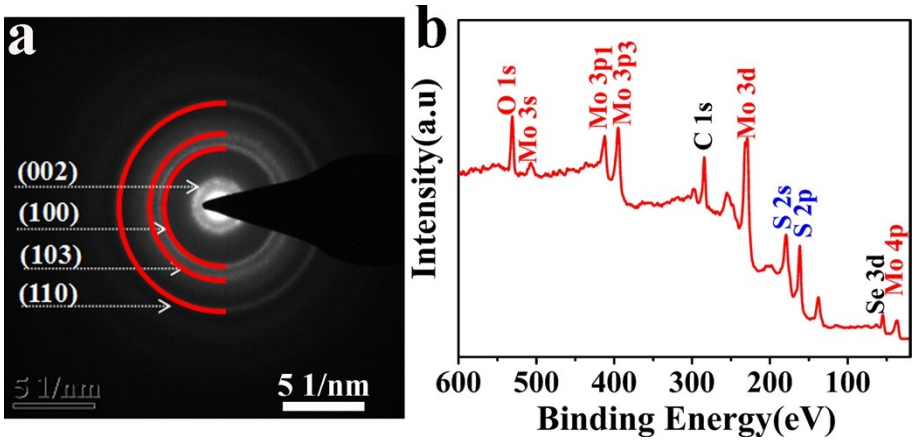

Figure S4 a,b) SAED pattern and XPS full spectra of the $MoS_{2(1-x)}Se_{2x}$ (x=0.25) nanosheets.

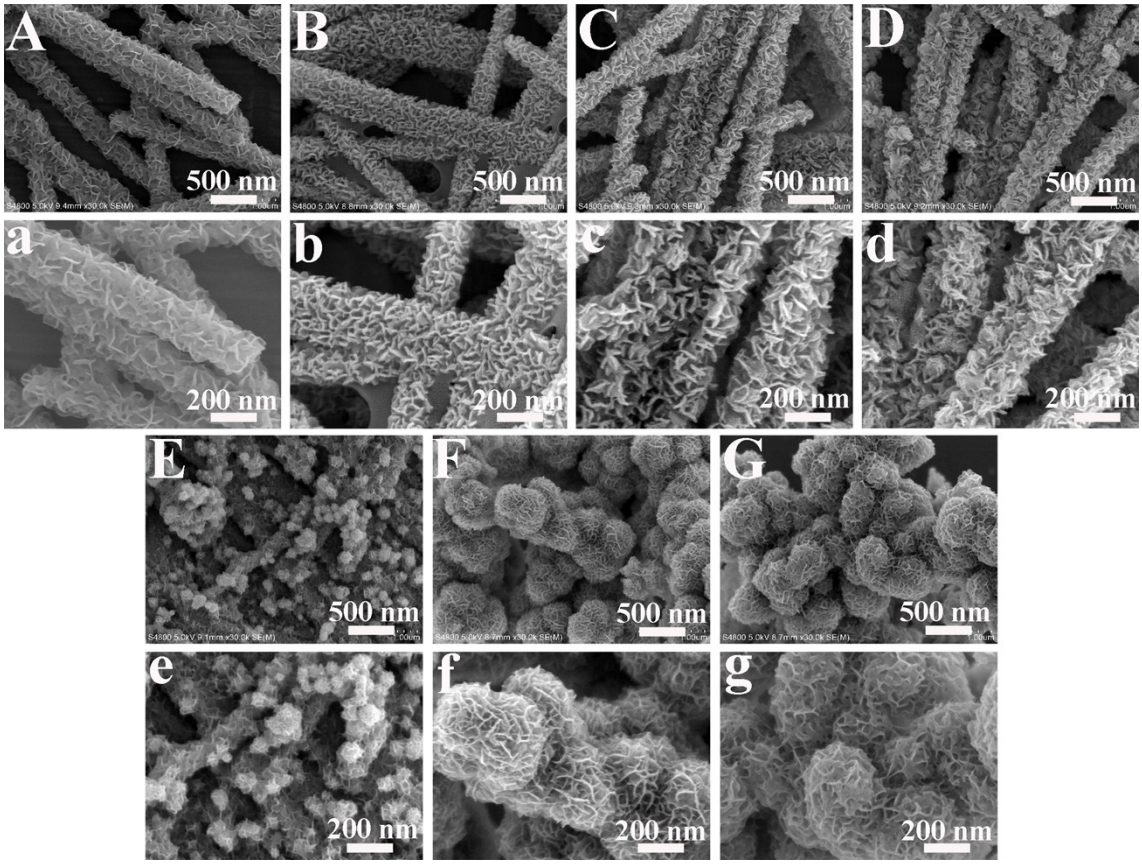

Figure S5 SEM images of $MoS_{2(1-x)}Se_{2x}$ nanosheets with different selenium content for A,a) x=0 (S/Se=2:0), B,b) x=0.05 (S/Se=19:1), C,c) x=0.2 (S/Se=4:1), D,d) x=0.25 (S/Se=3:1), E,e) x=0.35 (S/Se≈2:1), F,f) x=0.5 (S/Se=1:1) G,g) x=1 (S/Se=0:2).

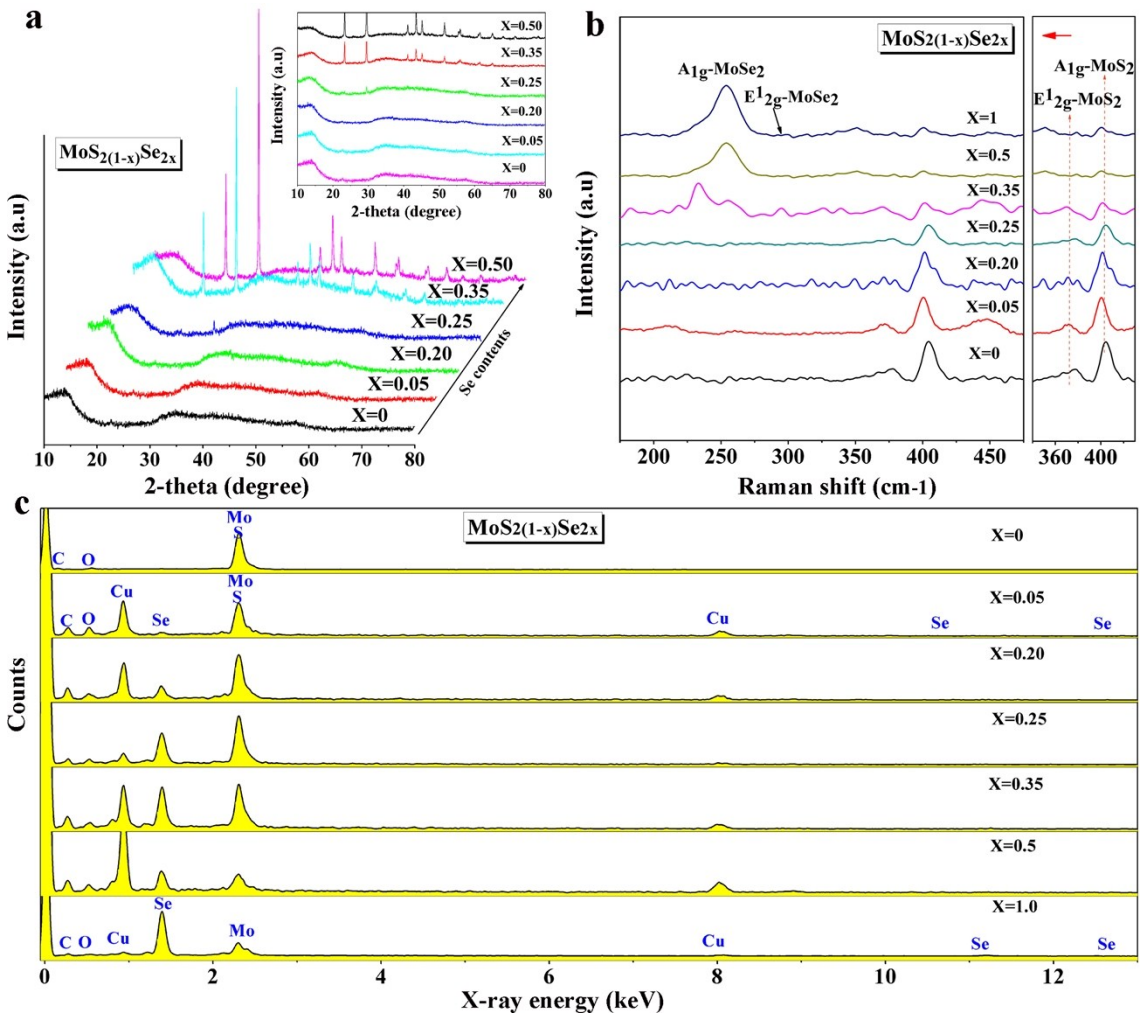

Figure S6 a) XRD, b) RS, c) EDX spectrum (C, O and Cu elements are coming from the Cu grid) of the different selenium content of the $MoS_{2(1-x)}Se_{2x}$ nanosheets.

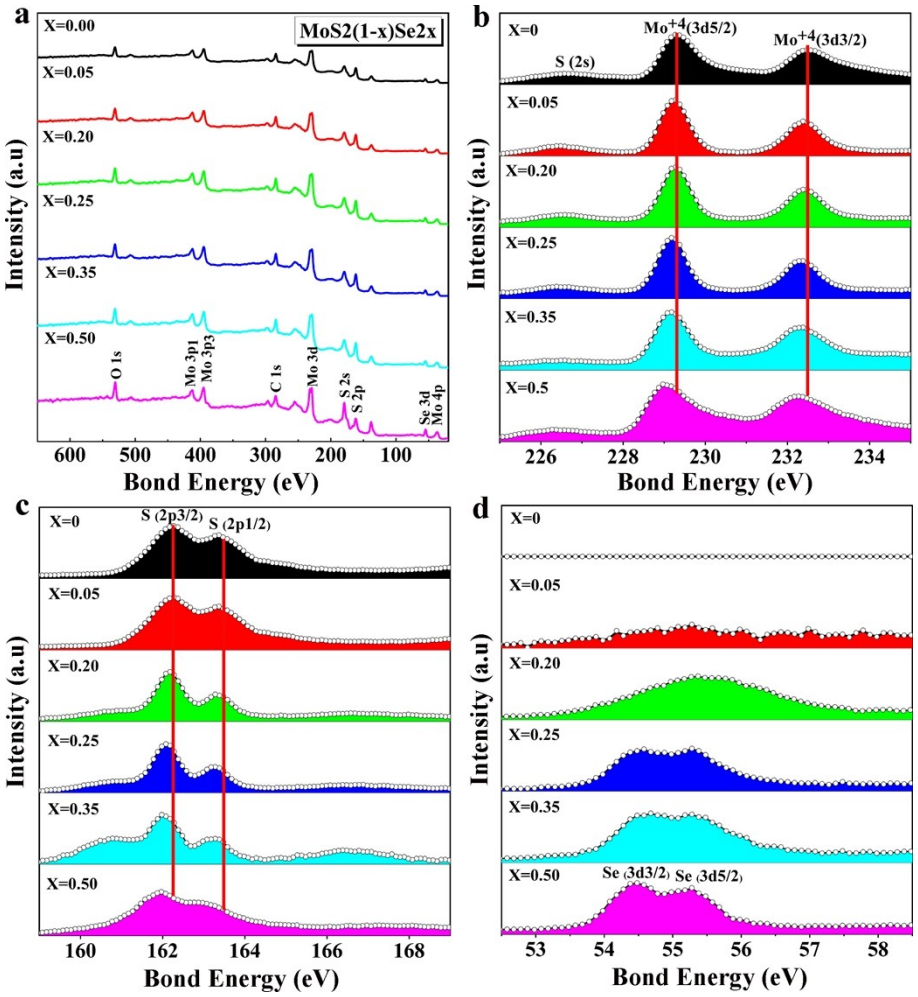

Figure S7 a) XPS full spectra and b-d) XPS high-resolution spectra Mo 3d, S 2p and Se 3d of the different selenium content of the $MoS_{2(1-x)}Se_{2x}$ nanosheets.

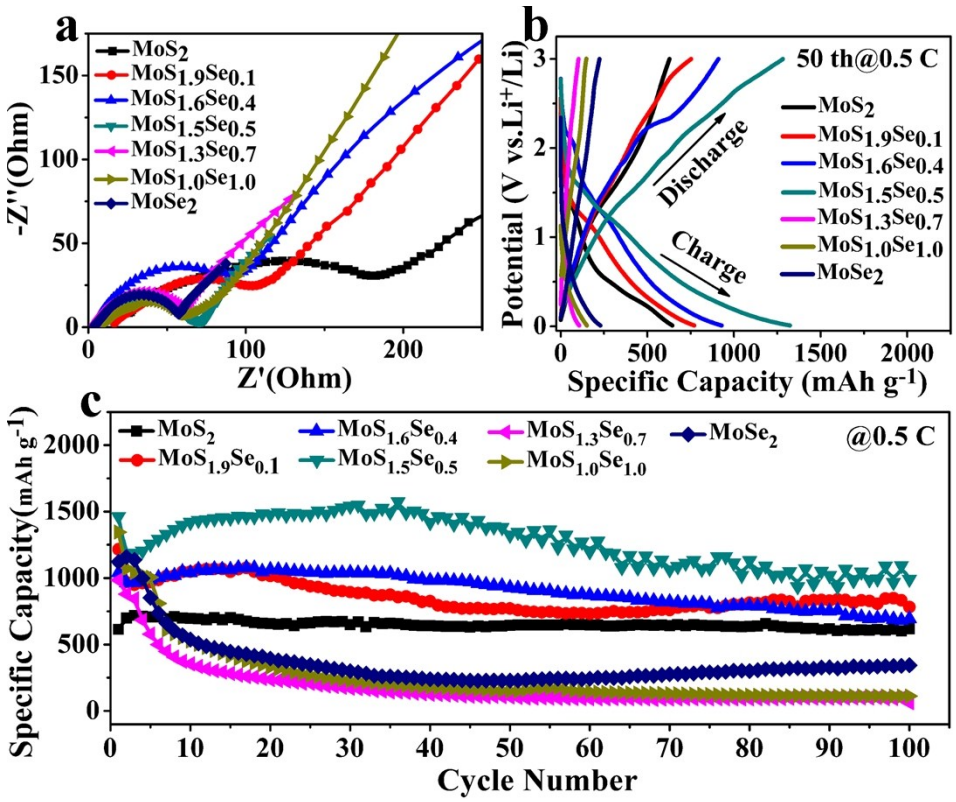

Figure S8 Electrochemical performance of different proportions of selenium content. a) AC impedance spectrum, b) Galvanostatic charge-discharge voltage profiles for the 50th cycles at a current density of 0.5C, c) Initial 100 cycling performance at 0.5C for $MoS_{2(1-x)}Se_{2x}$ nanosheets with different proportions of selenium content.

Table S1 Formation Energies (in eV) of the $MoS_{2(1-x)}Se_{2x}$ Alloys with Different Se Contents.

X	0	0.0625	0.1875	0.25	0.34375	0.5
Ef	0	0.56	1.78	2.38	3.38	4.96

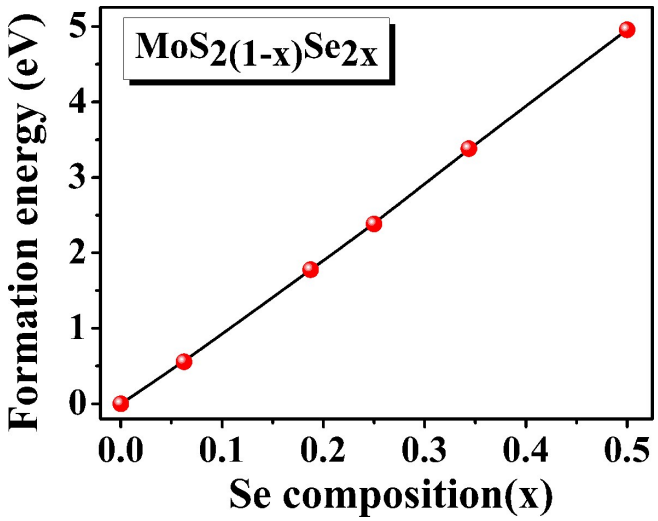

Figure S9 Formation energy (eV) change diagram of different selenium content.

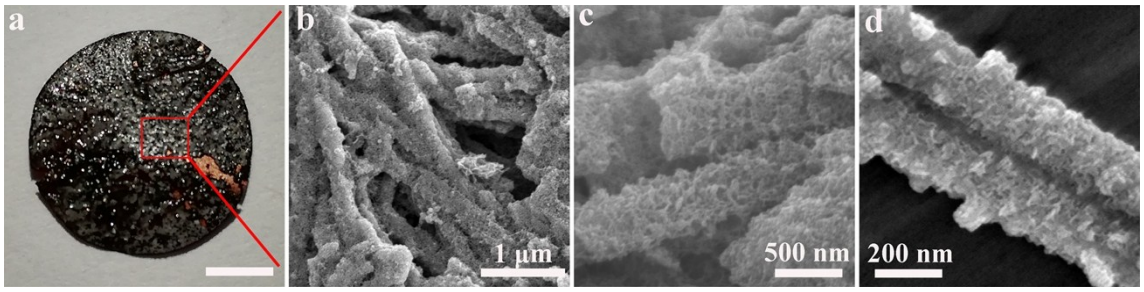

Figure S10 a-d) Camera photo and FESEM images of the $MoS_{2(1-x)}Se_{2x}$ (x=0.25) nanosheets after cycle, which proves the structure was robust enough and could still keep their structure even after 100 cycles.

Table S2 Summary of lithium-ion battery performance of the reported MoS_2-based electrode materials.

Electrodes	Method	Current density	Specific capacity	Ref
1T @2H MoS_2/carbon cloth	Solvothermal	2 A g^{-1}	510 mA h g^{-1} (after 500 cycles)	1
2H MoS_2/graphene	Lithium intercalation	0.4 A g^{-1}	450 mA h g^{-1} (over 500 cycles)	2
Carbon@MoS_2 tube sponges	Solvothermal	0.1 A g^{-1}	740 mA h g^{-1} (after 100 cycles)	3
2H MoS_2@carbon	PANI assisted hydrothermal	0.1 A g^{-1}	952.6 mA h g^{-1} (after 50 cycles)	4
MoS_2@MoO_3	Hydrothermal	0.1A g^{-1}	781 mA h g^{-1} (after 100 cycles)	5
Quasi-hollow MoS_2 microspheres encapsulated porous carbon	Hydrothermal	1 A g^{-1}	670 mA h g^{-1} (after 100 cycles)	6
Reduced graphene oxide/MoS_2 nanoflowers	Hydrothermal	0.5 A g^{-1}	680 mA h g^{-1} (after 250 cycles)	7
Carbon-sandwiched monolayered MoS_2	Hydrothermal	0.1 A g^{-1}	807 mA h g^{-1} (after 100 cycles)	8
C@MoS_2@C sandwiched hollow spheres	Template method	0.1C (C~670 mA h g^{-1})	856.7 mA h g^{-1} (after 100 cycles)	9
Hollow microsphere@onion-like solid nanosphere MoS_2	Hydrothermal	0.1 A g^{-1}	878 mA h g^{-1} (after 100 cycles)	10
MoS_2@carbon microspheres	Hydrothermal	1 A g^{-1}	650 mA h g^{-1} (after 300 cycles)	11
TiO_2@carbon@MoS_2 hierarchical nanotubes	Hydrothermal	0.2 A g^{-1}	770 mA h g^{-1} (after 100 cycles)	12
MoS_2@carbon hybridfibers	Hydrothermal	0.1 A g^{-1}	869 mA h g^{-1} (after 100 cycles)	13

N-rGO/MoS_2/N-rGO	Solvothermal	0.1 A g^{-1}	750 mA h g^{-1} (after 100 cycles)	14
		1 A g^{-1}	552 mA h g^{-1} (after 600 cycles)	
G/MoS_2	Exfoliation	0.1 A g^{-1}	931 mA h g^{-1} (after 100 cycles)	15
		1 A g^{-1}	340 mA h g^{-1} (after 300 cycles)	
$MoS_{2(1-x)}Se_{2x}$ (x=0.25) nanosheets	Etching method	0.5C (C=669 mA h g^{-1})	1000 mA h g^{-1} (after 100 cycles)	This work
		5C (C=669 mAh g^{-1})	500 mA h g^{-1} (after 350 cycles)	

References

1. T. Wang, C. Sun, M. Yang, G. Zhao, S. Wang, F. Ma, L. Zhang, Y. Shao, Y. Wu, B. Huang and X. Hao, *J. Alloys Compd.*, 2017, **716**, 112-118.
2. Y. Chao, R. Jalili, Y. Ge, C. Wang, T. Zheng, K. Shu and G. G. Wallace, *Adv. Funct. Mater.*, 2017, **27**, 1700234.
3. Y. Wang, Z. Ma, Y. Chen, M. Zou, M. Yousaf, Y. Yang, L. Yang, A. Cao and R. P. S. Han, *Adv. Mater*., 2016, **28**, 10175-10181.
4. L. Yang, S. Wang, J. Mao, J. Deng, Q. Gao, Y. Tang and O. G. Schmidt, *Adv. Mater*., 2013, **25**, 1180-1184.
5. H. Liu, X. Chen, L. Deng, M. Ding, J. Li and X. He, *J. Mater. Chem. A*, 2016, **4**, 17764-17772.
6. Z. Wan, J. Shao, J. Yun, H. Zheng, T. Gao, M. Shen, Q. Qu and H. Zheng, *Small*, 2014, **10**, 4975-4981.
7. F. Xiong, Z. Cai, L. Qu, P. Zhang, Z. Yuan, O. K. Asare, W. Xu, C. Lin and L. Mai, *ACS Appl. Mater. Interfaces*, 2015, **7**, 12625-12630.
8. J. Shao, Q. Qu, Z. Wan, T. Gao, Z. Zuo and H. Zheng, *ACS Appl. Mater. Interfaces*, 2015, **7**, 22927-22934.
9. Z. Li, A. Ottmann, T. Zhang, Q. Sun, H.-P. Meyer, Y. Vaynzof, J. Xiang and R. Klingeler, *J. Mater. Chem. A*, 2017, **5**, 3987-3994.
10. B. Guo, K. Yu, H. Song, H. Li, Y. Tan, H. Fu, C. Li, X. Lei and Z. Zhu, *Nanoscale*, 2016, **8**, 420-430.

11. Z. Bai, Y. Zhang, Y. Zhang, C. Guo and B. Tang, *Chem-Eur J*, 2015, **21**, 18187-18191.
12. S. Wang, B. Y. Guan, L. Yu and X. W. Lou, *Adv. Mater*., 2017, **29**, 1702724.
13. R. Zhou, J.-G. Wang, H. Liu, H. Liu, D. Jin, X. Liu, C. Shen, K. Xie and B. Wei, *Materials*, 2017, **10**, 174.
14. B. Chen, Y. Meng, F. He, E. Liu, C. Shi, C. He, L. Ma, Q. Li, J. Li and N. Zhao, *Nano Energy*, 2017, **41**, 154-163.
15. T. Wang, G. Zhao, C. Sun, L. Zhang, Y. Wu, X. Hao and Y. Shao, *Adv. Mater. Interfaces.*, 2017, **4**, 1601187.
16. Kresse, G.; Furthmüller, J., Efficiency of Ab-Initio Total Energy Calculations for Metals and Semiconductors Using a Plane-Wave Basis Set. *Computational materials science*, 1996, **6**, 15-50.
17. Kresse, G.; Hafner, J., Ab Initio Molecular Dynamics for Liquid Metals. *Physical Review B*, **1993**, **47**, 558.
18. Blöchl, P. E., Projector Augmented-Wave Method. *Physical review B*, 1994, **50**, 17953.
19. Perdew, J. P.; Chevary, J. A.; Vosko, S. H.; Jackson, K. A.; Pederson, M. R.; Singh, D. J.; Fiolhais, C., Atoms, Molecules, Solids, and Surfaces: Applications of the Generalized Gradient Approximation for Exchange and Correlation. *Physical Review B*, 1992, **46**, 6671.
20. Perdew, J. P.; Wang, Y., Accurate and Simple Analytic Representation of the Electron-Gas Correlation Energy. *Physical Review B,* 1992, **45**, 13244.
21. Monkhorst, H. J.; Pack, J. D., Special Points for Brillouin-Zone Integrations. *Physical review B*, 1976, **13**, 5188.